International Journal of Medical Toxicology & Legal Medicine Volume 27, No. 2S, 2024
e-ISSN: 0974-4614
p-ISSN: 0972-0448

Synthesis and Evaluation of Nanoparticles Formulations of Anti-Tubercular Drugs

Mahesh Kumar[1], Yogendra Singh[1], Arun Garg[1], Ashutosh Upadhyay[1],Girish Kumar[2], Prof (Dr) Tarun Virmani[2*]

[1]School of Pharmaceutical Sciences, MVN University, Palwal, Haryana 121105, India.
[2]Amity Institute of Pharmacy, Amity University, Greater Noida, Uttar Pradesh, 201308, India.

Received: 16.08.2024 Revised: 19.09.2024 Accepted: 23.10.2024

ABSTRACT
Aim: The purpose of this research was to prepare isoniazid loadedsolid lipid nanoparticles (SLNs) for oral administration aiming at improving the therapeutic efficiency in the treatment of tuberculosis. The isoniazid loaded SLNs were designed using glyceryldibehenateas a lipid component and tween 80 as surfactant by homogenization technique. Box-Behnken design was implemented to get optimized SLN formulation of isoniazid having lipid concentration, surfactant concentration, and homogenization speed as independent variables and particle size and entrapment efficiency as dependant variables. The Formulation having lipid concentration 100 mg, surfactant concentration 15 mg, and homogenization time of 15 minute was found optimized with particle size of 247.65 ± 1.2 nm and entrapment efficiency of 80.68 ± 3.2 %. The optimized formulation provided prolonged release of 89.94 ± 1.5% after 6 hours which was more than 90% within 1 hour for pure drug solution suggesting improved duration of action. These results suggested the improved therapeutic efficiency of SLN loaded with isoniazid which required pharmacokinetic and pharmacodynamic studies for further confirmation. The present study concluded that SLNs may be utilized to provide a more prolonged, enhanced release of the drugs without altering the dosage.

Keywords: Anti-tubercular, Controlled release, Mycobacterium tuberculosis, Nanotechnology, Tuberculosis.

1. INTRODUCTION

Mycobacterium tuberculosis, which causes TB, is a chronic infectious illness that has infected over a billion people globally. One-fourth of all known TB cases worldwide are reported each year in India, the second most populated nation in the world [1]. Around 10.6 million individuals were infected with tuberculosis (TB) worldwide in 2021[2]. Tuberculosis is also the largest cause of mortality among HIV (human immunodeficiency virus)-infected patients, as well as a significant cause of death due to antibiotic resistance[3]. According to the WHO Report 2019, around 1.6 million people die as a result of tuberculosis[4]. Furthermore, it affects one-third of the world's population in a dormant state. The Asian subcontinent has been hit the hardest, with India reporting the highest count of TB cases[5]. In addition to highlighting the need for the development of novel TB drug therapies, the growth of multidrug-resistant TB has also drawn attention to the shortcomings of the present conventional TB therapy, particularly the lengthy duration of the regimens and the issues with patient compliance [6]. These delivery methods offer continuous drug release, which may reduce the need for frequent high doses, as well as cutting-edge methods for delivering drugs to specific locations inside the host, enhancing therapeutic effects while avoiding systemic side effects[7][8].

In "Category-III" tuberculosis treatment, the first-line antitubercular medicines (ATDs) used were Rifampicin (RIF), Isoniazid (INH), and Pyrazinamide (PYZ). For oral administration in the initial phase, three doses of INH, RIF, and PYZ per week for two months were indicated by the specifically observed short course of treatment (DOTS) for category III[9]. These first-line antitubercular medications have several drawbacks, including hepatotoxicity, gastrointestinal disturbances, rashes, and drug resistance[10].Due to their many benefits over other innovative colloidal carriers, such as the protection of labile medicines, physical stability, superior tolerability, and controlled release, the ATDs encapsulated Poly (lactic-co-glycolic acid) (PLGA)and Solid lipid nanoparticles (SLNs) have been created as a drug delivery method [11]. Pharmaceutical researchers from all around the world are becoming more interested in the creation of PLGA and SLNs due to their benefits and superior tolerability when compared to other polymeric nanoparticles[12]. PLGA can be manufactured in almost any form and size and is soluble in common solvents. Hydrophobic drug loading into SLNs has demonstrated excellent therapeutic outcomes in some studies [13], and in certain investigations, the use of antibiotic-loaded nanoparticles even led to the complete eradication of M. tb[14]. For effective optimization and

characterization of SLNs, though, a consistent methodology is required. The most extensively used kind of particles are PLGA particles, and the expanded usage of PLGA nanoparticle-based drug delivery systems is promising because of their greater effectiveness and lower risk of side effects[15]. The most palatable response surface methodology for optimizing nanoparticulate formulation is central composite design (CCD)[16]. The CCD aids in lowering the expense of sophisticated and pricey analytical techniques as well as the associated numerical noise. Current anti-TB medications have been found to include a variety of colloidal drug carriers, and Blasi et al. presented an exhaustive and critical evaluation of contemporary formulations. Anisimovia et al. 2000 found that acrylate nanoparticles encapsulating isoniazid (INH), rifampicin (RIF), and streptomycin were as efficacious as or more so than the free medicines and that the nanoparticles increased intracellular drug concentrations in vitro[17]. This study focuses on the synthesis of two nanoparticles, SLN and PLG NPs loaded with 3 anti-tubercular drugs, Isoniazid, Rifampicin, and Pyrazinamide to check their stability and efficacy against the M. tb.

2. METHODOLOGY

2.1 Procurement of Chemicals

Isoniazid, Glyceryldibehenate, tween 80, phosphotungstic acid, popidium iodide were purchased from BR Chemicals, Faridabad. RAW 264.7 cell lines and hydrochloric acid of analytical grade were obtained from Sigma Chemicals.

2.2 Formulation of drug loaded SLNs

Glyceryldibehenate was used as the lipid component and for surfactant Tween 80 was used in the synthesis of SLN, which was accomplished using a “hot high shear homogenization (HSH) technique” as previously reported [18]. The lipid phase, in a nutshell, was melted at 10°C over its melting point. The melted lipid was then infused with isoniazid, rifampicin, and pyrazinamide until completely dissolved. To form the aqueous phase, Tween 80 was dissolved in filtered water and heated to approximately the same degree of temperature as the oil phase. The heated aqueous phase was then mixed with the lipid phase using a “high-shear laboratory mixer” at 12300 rpm for 10 minutes, maintaining the lipids' melting temperature. The heated nanoemulsion was ultimately allowed to cool with moderate agitation for five minutes to produce the SLN dispersions. Each formulation was evaluated in triplicates. The finished dispersions were packed in sterile glass, secured with the help of aluminum seals and bromobutyl rubber stoppers, and kept at 5°C until use[19].

2.3 Optimization of SLNs using box-behnken

Box-Behnken design (BBD) was used to optimize SLNs components using Design Expert software, Stat-Ease, Minneapolis, MN, USA. Independent variables such as lipid concentration (mg), surfactant concentration (%), and homogenization time (min) were chosen based on their potential impact on dependent variables such as particle size (Y1; nm), and entrapment efficiency (Y2;%).The design proposed 17 formulation runs[20]. Table 1 summarizes the independent and dependent variables, including their respective levels.

Table 1: Independent variables with their levels and dependent variables

Independent variables	Levels		
	High level (1)	Medium (0)	Low level (-1)
A= Lipid concentration (mg)	200	150	100
B= Surfactant concentration (%)	15	10	5
C= Homogenization time (Min)	20	15	10
Dependent variables Y1: Particle size (nm) Y2: Entrapment efficiency (%)			

2.4 Characterization of optimized SLN formulation

2.4.1 Particle size, distribution, and surface charge

Using photon correlation spectroscopy, the z-average size of nanoparticles was calculated. Particle size, zeta potential, and PDI were calculated using the Zetasizer. Re-dispersion of the lyophilized isoniazidloaded SLNs (2 milligram) in double-distilled water (5 millilitre). The cuvette was filled with the diluted sample, heated to 25°C, and seen at a 90° angle[21].

2.4.2 Drug loading and entrapment efficiency

Size exclusion chromatography on Sephadex G-25/PD-10 columns were used to extract the isoniazid loading from the SLN dispersions after they were prepared. Centrifugation was used to separate the supernatant, which included the isoniazid loaded SLN. In the aqueous phase, the concentration of the free drug was calculated using UV-Visible spectrophotometry using a microplate spectrophotometer reader[22].

The following formulae were used to compute the drugs EE and DL:

$$EE(\%) = \frac{W_{loaded\ drug}}{W_{initial\ drug}} \times 100$$

$$DL(\%) = \frac{W_{loaded\ drug}}{W_{lipid}} \times 100$$

where,
"$W_{initial}$drug =weight of the drug used,
W_{loaded} drug = weight of encapsulated drug that was detected in the supernatant after nanoparticle solubilization, purification, and centrifugation.
W_{lipid}= weight of the lipid vehicle".

2.4.3 Morphological analysis
TEM (Transmission electron microscopes) was used to analyze the morphology of optimized SLN formulation. For observation, the samples were mounted on copper racks lined with carbon membranes, and they were dyed for two minutes with phosphotungstic acid at a 2 percent (w/v) concentration. Following that, they were examined at 120 kV using a Microscope, and photos were taken using a GatanOrius camera[16].

2.4.4Differential scanning calorimetry (DSC) studies
Thermal data analyses of DSC thermograms of pure isoniazid and isoniazid loaded lyophilized samples were recorded using a differential scanning calorimeter. Accurately weighed samples were heated in alumina pans at a predetermined rate of 10 degree Celsius per min under nitrogen at a flow rate of 40 millilitres per min. The temperature range covered was 25 to 400 degree Celsius. The equipment was calibrated before the sample charging using indium as a calibration reference[24].

2.4.5Fourier Transform Infrared Spectroscopy
An FTIR spectrophotometer was used to record infrared (IR) spectroscopy measurements of the isoniazid and optimized SLN formulation of isoniazid to determine the compatibility. For two minutes, the potassium bromide pellet technique was used at a hydrostatic pressure of 5 tones/cm^2, and the background spectrum was taken under the same circumstances. Each spectrum was created using 16 single average scans with a spectral resolution of 2cm^{-1} that were acquired in the 400–4000cm^{-1} range[25].

2.5 In vitro Dissolution studies
The release research was carried out utilizing the dialysis sack method with a DO405 dialysis membrane (Sigma, Germany). Five milliliters of formulation were placed in a dialysis membrane and immersed in 50 milliliters of phosphate buffer solution (pH 7.4). Two mL samples were taken at specified intervals, and the drug concentration was detected at 263 nm with a UV spectrophotometer (Shimadzu, Japan). Dilution of removed samples was performed when needed[10].
Different kinetic models, including zero order and first order, were used to match the in vitro drug release data of optimized isoniazid-loaded SLNs. The in vitro release data was fitted to the models of Higuchi and Korsmeyer-Peppas to better understand the drug release process. The kinetics and mechanism of drug release were determined using the greatest correlation coefficient (r2) values.

2.6 In vitro cell viability studies
By using a modified version of the MTT (3-(4, 5-dimethyl thiazol-2yl)-2, 5-diphenyl tetrazolium bromide) test method, the cytotoxicity of the pure isoniazid and SLN formulation of isoniazid was examined on the murine macrophage cell line RAW 264.7 (ATCC®TIB71TM). 96-well plates with 100µL of DMEM supplemented with 10% FBS were used to plate the RAW 264.7 cells at a density of 1 ×105 cells per well. After overnight incubation at 37°C in a 5% CO2 incubator, the medium was withdrawn, and 100 L of DMEM + 10% FBS was then added with various amounts of synthetic inhibitor. Additionally, as positive controls for cytotoxic testing, isoniazid, and SLNs containing isoniazid were used. The cells were then treated with MTT dye (5 mg in 10 mL of 1 X PBS) at a concentration of 10 L per well and incubated at room temperature in the dark for 4 h to enable the development of formazan crystals after being incubated for 20 hours. Crystals created in this way were entirely dissolved in 100 µL of DMSO after 4 hours. DMSO was used as a blank in a microplate reader to read the optical density (OD) readings at 570 nm. The relationship between the relative cell viability and the concentration of inhibitors was shown on a common graph[26].

$$\text{Cell viability (\%)} = \frac{\text{Test OD}}{\text{Control OD}} \times 100$$

3. RESULT

3.1 Optimization of drugs by using the factorial design method

A total of 17 various formulations suggested by BBD were fabricated having the values of particle size (Y1) and entrapment efficiency (Y2) in the range of 247.65-320.12 nm and 74.32-92.03% respectively. To know the quantitative relationship of all independent factors on dependant factors, the software provided polynomial equations for each:

Particle Size (Y1) = +287.65 +18.68*A -15.58*B -1.51*C +7.51*AB -5.89*AC -5.81*BC EQ.1

Entrapment efficiency (Y2) = +83.65 +5.77*A -1.35*B +1.45*C Eq. 2

Equation 1 shows the effect of lipid concentration (A), surfactant concentration (B), and homogenization time (C) on the particle size (Y1). It shows that increase in the concentration of lipid, the particle size also increases but the increase in concentration of surfactant and homogenization time causes reduction in particle size. The combination of lipid concentration and surfactant concentration had positive effect while combination of surfactant concentration and homogenization time had negative effect on particle size. The results of equations were supported by the 3D graphs generated by the software (Figure 1).

Equation 2 shows that entrapment efficiency increases with increase in concentration of lipid and homogenization time whilst it decreases with increase in concentration of surfactant.

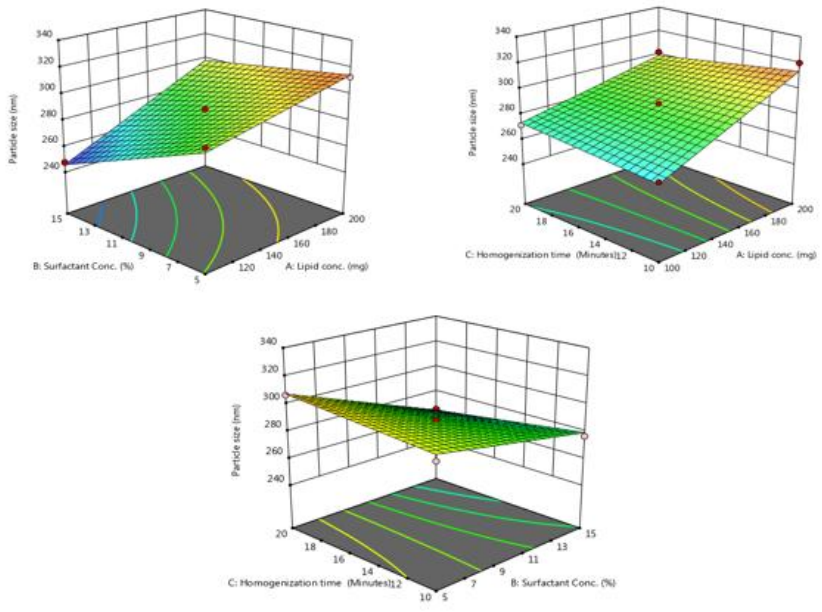

Figure 1: 3D graphs showing interactive effects of independent variables on particle size

3.2 Characterization of optimized SLN formulation

3.2.1Particle size, distribution, and zeta potential

The particle size of optimized SLN formulation of isoniazid was found to be 247.65 ± 1.2 nm. The reduced size of the SLNs provides increased surface area resulting in improved solubility and permeability and hence activity. The polydispersity index of SLNs loaded with isoniazid was observed 0.355±0.04demonstrating the narrow size distribution of the nanoparticles. The zeta potential of SLNs loaded with isoniazid was found −42.20 ± 1.32mV as represented in the Figure 2. The zeta potential of rifampicin and pyrazinamide loaded SLNs was higher than +30 mV and -30 mV indicating better stability of the formulation.

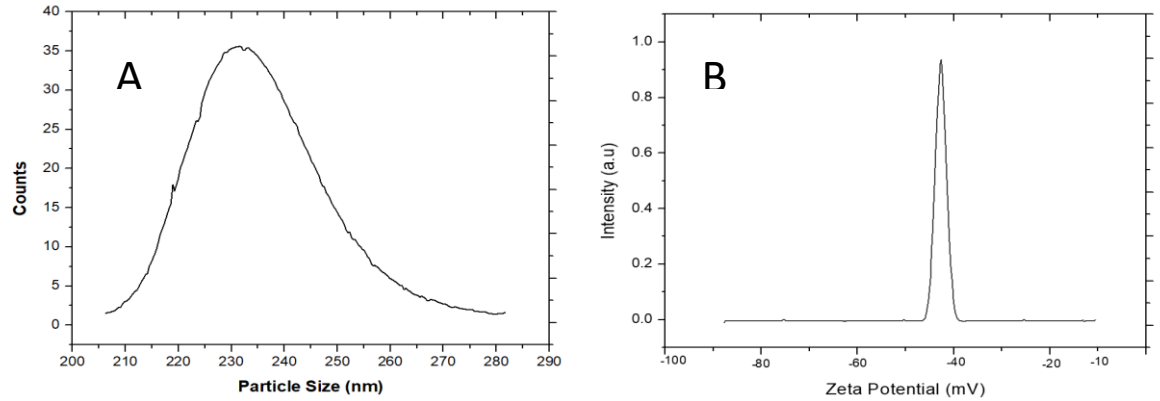

Figure 2: A represents particle size and B represents Zeta potential of optimized SLN of isoniazid

3.2.2 Drug loading and encapsulation efficiency

The loading and entrapment efficiency of isoniazid in SLNs was observed 663±45 mg/g and 80.68 ± 3.2% respectively. The results for drug loading and encapsulation efficiency depicted that isoniazid loaded SLNs had noteworthy outcomes.

3.2.3 Morphological analysis

The findings of TEM analysis for optimized SLNs of isoniazid have been represented in the Figure 3 which revealed spherical shape of the nanoparticles along with size in nanometric range. In addition, the aggregation of particles was absent depicting improved stability of the SLNs.

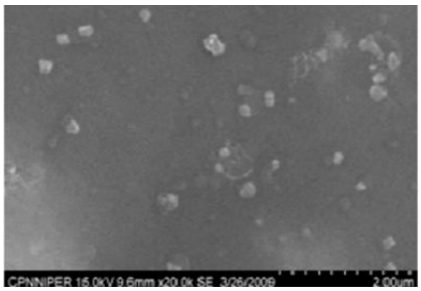

Figure 3: TEM image of optimized SLN formulation of isoniazid

3.2.4Differential scanning calorimetry (DSC)

The pure isoniazid displayed a single, sharp exothermic peak at about 168.5 degree Celsius (H = 260.1 Joules per gram), while the peak was disappeared in case of optimized SLN formulation of isoniazid (Figure 4). It could be due to conversion of crystalline form of isoniazid into the amorphous form owing to formulation of SLN.

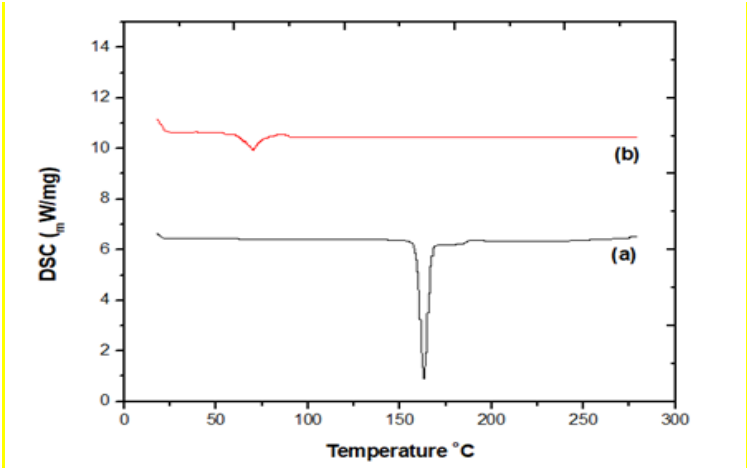

Figure 4: (a) depicts thermogram of pure isoniazid and (b) depicts thermogram of optimized SLN of isoniazid

3.2.5. Fourier Transform Infrared Spectroscopy

The results of FTIR analysis of SLNs loaded with isoniazid has been illustrated in the Figure 5. The hydrazide group's N-H stretching vibrations were attributed to the distinctive isoniazid FTIR bands at 3299 and 3103 cm-1 which confirmed the absence of incompatibility in the SLN of isoniazid. Moreover, the spectrum of pure isoniazid was approximately same as that of optimized SLN formulation of isoniazid.

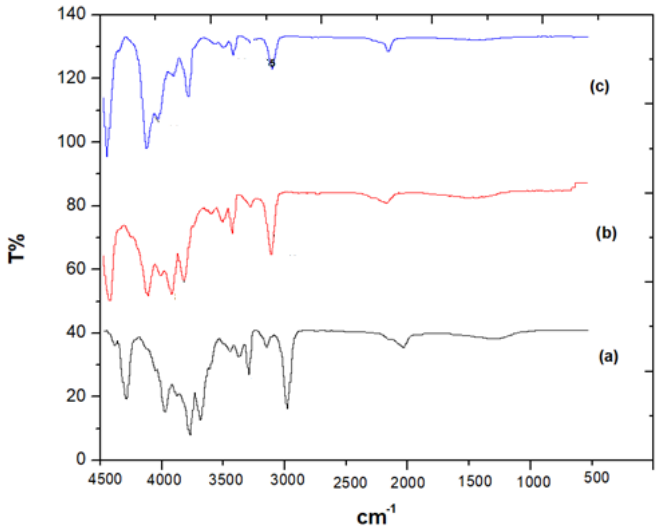

Figure 5. Fourier transmission infrared spectrum of (a) pure isoniazid (b) Physical mixture of isoniazid and (c) optimized SLN of isoniazid

3.3. In vitro dissolution studies

The in vitro drug release of optimized SLN verses isoniazid solution has been illustrated in Figure 7. The pure isoniazid solution exhibited maximum drug release of 91.64 ± 1.5 % within one hour whilst it was only 39.31 ± 2.3% for optimized SLN of isoniazid. Optimized SLN formulation of isoniazid provided maximum release of 89.94 ± 1.5% after 6 hours revealing the prolonged release of drug from optimized SLN than pure drug solution.

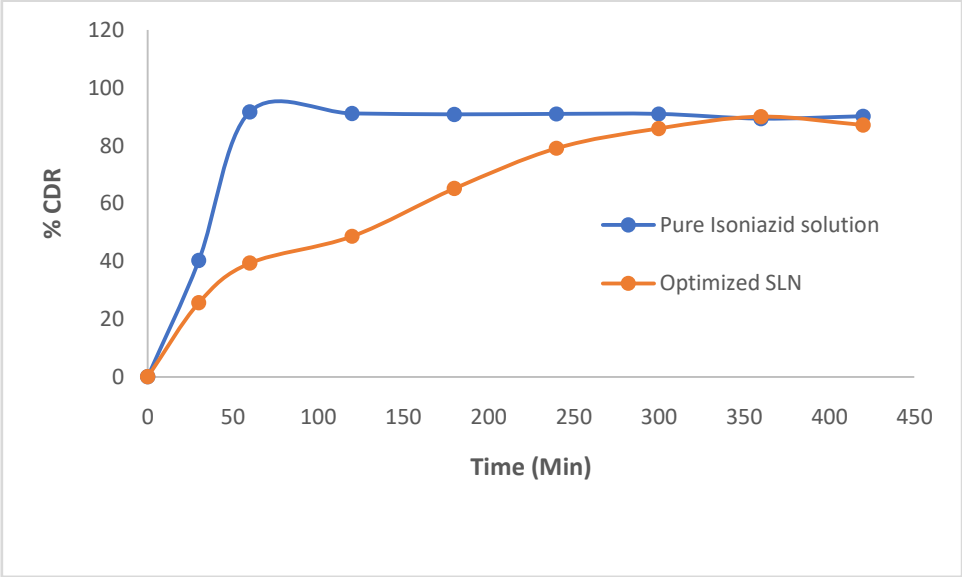

Figure 6. Graphical representation of in vitro dissolution rate of isoniazid loaded SLN

3.4. In vitro cell viability study

The Raw 264.7 cell viability after being exposed to free isoniazid at a 20 mM concentration of drug-loaded SLNs was lower than 90% which depicts the safety of SLN of isoniazid (Figure 6).

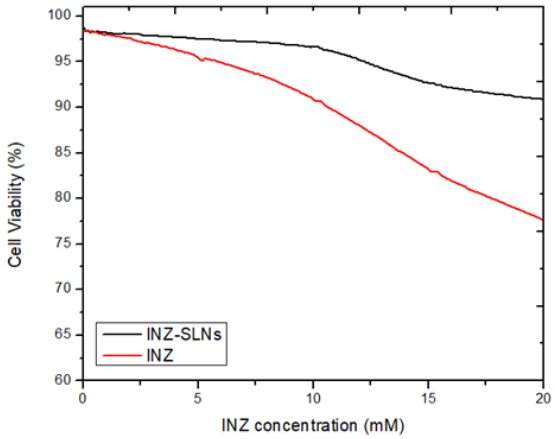

Figure 7: Change of cell lines Raw 264.7, cell viability after 24 hours treatment with free drug loaded isoniazid SLN

CONCLUSION

Isoniazid loaded SLNs were successfully prepared and optimized using box-behnken design to improve the therapeutic efficiency in the treatment of tuberculosis. The optimized SLN formulation of isoniazid was found to have particle size, polydispersity index, and zeta potential of 247.65 ± 1.2 nm, 0.355±0.04, and −42.20 ± 1.32 mV respectively. The optimized formulation exhibited 89.94 ± 1.5% drug release within 6 hours while pure isoniazid solution exhibited 91.64 ± 1.5 % release only after 1 hour. The drug release study revealed the prolonged release of the isoniazid which could be attributed to the reduction in adverse effects of the drug along with pronged duration of action. Additional studies on pharmacokinetics and pharmacodynamics will be done to confirm the drug's bioavailability and in vivo potential, following the observed results.

REFERENCE

1. M. Kumar et al., “Nanocarriers in Tuberculosis Treatment: Challenges and Delivery Strategies,” Pharmaceuticals, vol. 16, no. 10, Art. no. 10, Oct. 2023, doi: 10.3390/ph16101360.
2. A. A. Khatib, S. Hassanein, M. Almari, M. Koubar, and S. Fakhreddine, “Tuberculosis morbidity and mortality during the COVID-19 pandemic: a life-threatening complex challenge,” Front. Cell. Infect. Microbiol., vol. 14, p. 1423081, Oct. 2024, doi: 10.3389/fcimb.2024.1423081.
3. S. Kumar et al., “Synthesis, Anticancer, and Antimicrobial Evaluation of Integerrimide-A,” BioMed Res. Int., vol. 2023, no. 1, p. 9289141, 2023, doi: 10.1155/2023/9289141.
4. D. Dhamnetiya, P. Patel, R. P. Jha, N. Shri, M. Singh, and K. Bhattacharyya, “Trends in incidence and mortality of tuberculosis in India over past three decades: a joinpoint and age–period–cohort analysis,” BMC Pulm. Med., vol. 21, no. 1, p. 375, Nov. 2021, doi: 10.1186/s12890-021-01740-y.
5. K. Sharma et al., “Exploring novel antitubercular agents: Innovative design of 2,3-diaryl-quinoxalines targeting DprE1 for effective tuberculosis treatment,” Open Chem., vol. 22, no. 1, Jan. 2024, doi: 10.1515/chem-2024-0086.
6. “Treatment strategies for MDR-TB and XDR-TB,” in Companion Handbook to the WHO Guidelines for the Programmatic Management of Drug-Resistant Tuberculosis, World Health Organization, 2014. Accessed: Nov. 12, 2024. [Online]. Available: https://www.ncbi.nlm.nih.gov/books/NBK247431/
7. G. Kumar, T. Virmani, A. Sharma, R. Virmani, and K. Pathak, “Chapter 14 - Nanoparticulate drug delivery systems for colonic disorders,” in Advanced Drug Delivery Systems for Colonic Disorders, H. Dureja, R. Loebenberg, S. K. Singh, M. Dhanasekaran, and K. Dua, Eds., Academic Press, 2024, pp. 317–344. doi: 10.1016/B978-0-443-14044-0.00009-0.
8. G. Kumar, T. Virmani, A. Sharma, R. Virmani, and K. Pathak, “Synbiotics in Oral Drug Delivery,” in Synbiotics in Human Health: Biology to Drug Delivery, K. Dua, Ed., Singapore: Springer Nature, 2024, pp. 413–433. doi: 10.1007/978-981-99-5575-6_20.
9. S. Khatak et al., “Solid lipid nanoparticles containing anti-tubercular drugs attenuate the Mycobacterium marinum infection,” Tuberculosis, vol. 125, p. 102008, Dec. 2020, doi: 10.1016/j.tube.2020.102008.
10. G. Kumar, R. K. Khar, T. Virmani, V. Jogpal, and R. Virmani, “Comparative Evaluation of Fast Dissolving Tablet of Atorvastatin Calcium using Natural and Synthetic Super Disintegrating Agents,” Res. J. Pharm. Technol., vol. 11, no. 11, pp. 5001–5007, Nov. 2018, doi: 10.5958/0974-360X.2018.00912.5.
11. J. Bharti Sharma et al., “Statistical optimization of tetrahydrocurcumin loaded solid lipid nanoparticles using Box Behnken design in the management of streptozotocin-induced diabetes mellitus,” Saudi Pharm. J., vol. 31, no. 9, p. 101727, Sep. 2023, doi: 10.1016/j.jsps.2023.101727.

12. G. Kumar, T. Virmani, A. Sharma, and K. Pathak, “Codelivery of Phytochemicals with Conventional Anticancer Drugs in Form of Nanocarriers,” Pharmaceutics, vol. 15, no. 3, Art. no. 3, Mar. 2023, doi: 10.3390/pharmaceutics15030889.
13. T. Virmani, G. Kumar, R. Virmani, A. Sharma, and K. Pathak, “Nanocarrier-Based Approaches to Combat Chronic Obstructive Pulmonary Disease,” Nanomed., vol. 17, no. 24, pp. 1833–1854, Oct. 2022, doi: 10.2217/nnm-2021-0403.
14. A. Sharma, T. Singh, D. Pathak, T. Virmani, G. Kumar, and A. Alhalmi, “Antidepressive-Like Effect of Aegle marmelos Leaf Extract in Chronic Unpredictable Mild Stress-Induced Depression-Like Behaviour in Rats,” BioMed Res. Int., vol. 2022, p. 6479953, 2022, doi: 10.1155/2022/6479953.
15. T. Virmani et al., “Amelioration of Cancer Employing Chitosan, Its Derivatives, and Chitosan-Based Nanoparticles: Recent Updates,” Polymers, vol. 15, no. 13, Art. no. 13, Jan. 2023, doi: 10.3390/polym15132928.
16. G. Kumar, T. Virmani, K. Pathak, O. A. Kamaly, and A. Saleh, “Central Composite Design Implemented Azilsartan Medoxomil Loaded Nanoemulsion to Improve Its Aqueous Solubility and Intestinal Permeability: In Vitro and Ex Vivo Evaluation,” Pharm. Basel Switz., vol. 15, no. 11, p. 1343, Oct. 2022, doi: 10.3390/ph15111343.
17. S. M. D’Addio, V. M. Reddy, Y. Liu, P. J. Sinko, L. Einck, and R. K. Prud’homme, “Antitubercular Nanocarrier Combination Therapy: Formulation Strategies and in Vitro Efficacy for Rifampicin and SQ641,” Mol. Pharm., vol. 12, no. 5, p. 1554, Mar. 2015, doi: 10.1021/mp5008663.
18. P. Mura, F. Maestrelli, M. D’Ambrosio, C. Luceri, and M. Cirri, “Evaluation and Comparison of Solid Lipid Nanoparticles (SLNs) and Nanostructured Lipid Carriers (NLCs) as Vectors to Develop Hydrochlorothiazide Effective and Safe Pediatric Oral Liquid Formulations,” Pharmaceutics, vol. 13, no. 4, Art. no. 4, Apr. 2021, doi: 10.3390/pharmaceutics13040437.
19. R. Osanlou, M. Emtyazjoo, A. Banaei, M. A. Hesarinejad, and F. Ashrafi, “Preparation of solid lipid nanoparticles and nanostructured lipid carriers containing zeaxanthin and evaluation of physicochemical properties,” Colloids Surf. Physicochem. Eng. Asp., vol. 641, p. 128588, May 2022, doi: 10.1016/j.colsurfa.2022.128588.
20. T. Virmani, S. Singh, and K. Kohli, “Nanoemulsion System for Improvement of Raspberry Ketone Oral Bioavailability,” Indo Glob. J. Pharm. Sci., vol. 10, pp. 33–42, Oct. 2020, doi: 10.35652/IGJPS.2020.10105.
21. L. Wang et al., “Paclitaxel and naringenin-loaded solid lipid nanoparticles surface modified with cyclic peptides with improved tumor targeting ability in glioblastoma multiforme,” Biomed. Pharmacother., vol. 138, p. 111461, Jun. 2021, doi: 10.1016/j.biopha.2021.111461.
22. G. Mahlawat, T. Virmani, and M. Arif, “Enhancement Of Therapeutic Action Of Anti-Hyperlipidemic Drugs By Using A Novel Nanosuspension-Based Approach,” Int. J. Pharm. Sci. Res., vol. 15, p. 1679, Apr. 2023, doi: 10.13040/IJPSR.0975-8232.14(4).1679-90.
23. M. Silva-Abreu, E. Miralles, C. S. Kamma-Lorger, M. Espina, M. L. García, and A. C. Calpena, “Stabilization by Nano Spray Dryer of Pioglitazone Polymeric Nanosystems: Development, In Vivo, Ex Vivo and Synchrotron Analysis,” Pharmaceutics, vol. 13, no. 11, p. 1751, Oct. 2021, doi: 10.3390/pharmaceutics13111751.
24. S. Ahalwat et al., “Mannose-Functionalized Isoniazid-Loaded Nanostructured Lipid Carriers for Pulmonary Delivery: In Vitro Prospects and In Vivo Therapeutic Efficacy Assessment,” Pharmaceuticals, vol. 16, no. 8, Art. no. 8, Aug. 2023, doi: 10.3390/ph16081108.
25. S. Dhir et al., “Amomum subulatum Fruit Extract Mediated Green Synthesis of Silver and Copper Oxide Nanoparticles: Synthesis, Characterization, Antibacterial and Anticancer Activities,” Processes, vol. 11, no. 9, Art. no. 9, Sep. 2023, doi: 10.3390/pr11092698.
26. M. A. Rahim et al., “In vitro anti-tuberculosis effect of probiotic Lacticaseibacillus rhamnosus PMC203 isolated from vaginal microbiota,” Sci. Rep., vol. 12, no. 1, p. 8290, May 2022, doi: 10.1038/s41598-022-12413-z.